

# TR-MOT: Multi-Object Tracking by Reference

Mingfei Chen<sup>1,3</sup> Yue Liao<sup>2</sup> Si Liu<sup>2</sup> Fei Wang<sup>3</sup> Jenq-Neng Hwang<sup>1</sup>

<sup>1</sup> University of Washington

<sup>2</sup> Institute of Artificial Intelligence, Beihang University <sup>3</sup> SenseTime Research

## Abstract

Multi-object Tracking (MOT) generally can be split into two sub-tasks, i.e., detection and association. Many previous methods follow the tracking by detection paradigm, which first obtain detections at each frame and then associate them between adjacent frames. Though with an impressive performance by utilizing a strong detector, it will degrade their detection and association performance under scenes with many occlusions and large motion if not using temporal information. In this paper, we propose a novel Reference Search (RS) module to provide a more reliable association based on the deformable transformer structure, which is natural to learn the feature alignment for each object among frames. RS takes previous detected results as references to aggregate the corresponding features from the combined features of the adjacent frames and makes a one-to-one track state prediction for each reference in parallel. Therefore, RS can attain a reliable association coping with unexpected motions by leveraging visual temporal features while maintaining the strong detection performance by decoupling from the detector. Our RS module can also be compatible with the structure of the other tracking by detection frameworks. Furthermore, we propose a joint training strategy and an effective matching pipeline for our online MOT framework with the RS module. Our method achieves competitive results on MOT17 and MOT20 datasets.

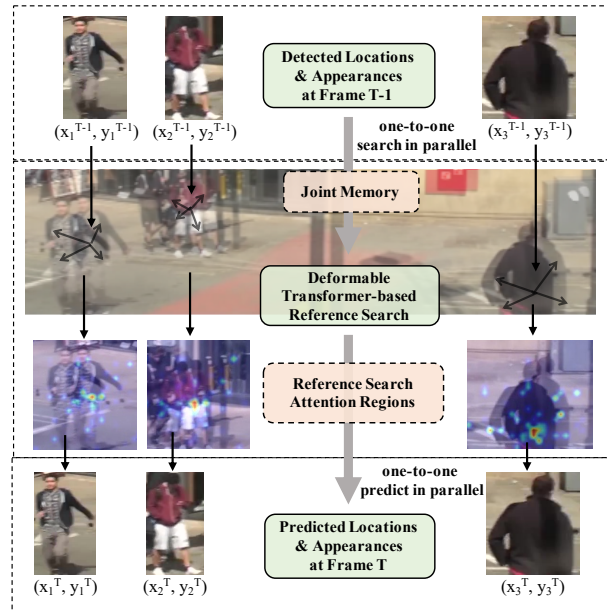


Figure 1. In Reference Search (RS), track locations and appearances at the previous frame are utilized as references to aggregate corresponding features from joint memory (feature summation of adjacent frames), and then predict the track states at the current frame one-to-one in parallel for association. RS can cope with appearance changes and erratic motions by leveraging temporal information and focusing on feature alignments among frames.

## 1. Introduction

Multi-object Tracking (MOT), an essential and practical task in video analysis, benefits many applications, e.g., autonomous driving and smart city. MOT aims to estimate the trajectory of objects with the same identity based on a video sequence that contains multiple objects. MOT generally can be split into two sub-tasks, i.e., detection and association. However, these two tasks are very different, where one is location-aware, and the other is identity-aware. Therefore, one challenge for MOT is how to extract suitable features in a general framework for these two tasks, the focus of which is very different in feature learning. Another challenge is

how to associate two objects with the unpredictable motion of the objects or cameras across two frames.

Conventional methods for MOT are mainly following the *tracking by detection* [15, 28, 32] and *joint tracking and detection* [22, 23] paradigms. Most previous *tracking by detection* methods first detect all objects and then associate them with previous tracks based on the appearance similarity and location overlap. If without learnt association based on visual temporal information, it will degrade their detection and association performance under scenes with many occlusions or large motions. *Joint detection and tracking* methods jointly learn detection and association, aggregate features from several adjacent frames to simultaneously predict

locations of the associated objects with the same identity at these frames. However, the strong coupling structure of detection and association is easily to overlook the different focuses of these two tasks.

In this paper, we propose a deformable transformer-based Reference Search (RS) method to achieve a more reliable association while maintaining the strong detection performance in the tracking by detection paradigm. For tracking at frame  $T$ , we perform detection only based on the features from frame  $T$ , and further associate the new detections to the existing tracks, whose current states, including the locations and appearance embeddings, will then be updated from combined features of the frame  $T$  and frame  $T - 1$  by using RS. Specifically, as Fig 1, in the RS module, track locations at the previous frame are utilized as the reference point set to aggregate the corresponding features with deformable co-attention from the two adjacent frames. Correspondingly, we introduce a novel joint training strategy and an effective matching pipeline for our framework with the RS module.

We argue that our TR-MOT has the following characteristics and advantages comparing to previous methods. We first discuss the MOT methods, which utilize visual temporal information to predict association based on a CNN structure such as CenterTrack [41], ChainedTracker [23] and TubeTK [22]. Unlike these previous methods, considering locations of other tracks to have a minor effect on the state prediction for this track, we leverage a more focused set-to-set transformer structure, which is more natural to make a one-to-one state prediction for each previous track in parallel. Moreover, our track state prediction is decoupled from detection and thus less limited by detection-related features. We then distinguish our TR-MOT from some recent transformer-based MOT methods [20, 27, 35, 37]. Such transformer-based trackers utilize the detection-related object features in the transformer-based detector to associate objects in other frames. Though attaining impressive detection accuracy, this manner is less reliable for association, because the learnt object features are highly specialized for the detection task, and thus may degrade the association ability. Decoupling from detection, our RS module only takes detection results as location references to learn the feature alignments based on visual temporal information. Without extra relationship modelling, our RS module can also be compatible with other tracking by detection framework structures, predicting new location and appearance embedding of each previously detected track more reliably for the later association.

Our contributions can be mainly summarized as three aspects: 1) We design an effective Reference Search (RS) module for the association, which utilizes the previous track states as references to make a parallel one-to-one state propagation for each existing track based on visual temporal fea-

tures. 2) We propose an online MOT framework (TR-MOT) that decouples the detection and association process, including a reliable matching pipeline compatible with RS and the corresponding joint training strategy. 3) Our TR-MOT achieves competitive performance on the MOT dataset, and ablation studies verify the effectiveness of our main designs.

## 2. Related Work

**Tracking by detection.** The methods in the tracking by detection category [15, 19, 28, 31, 32, 36, 39, 42] break the MOT task into two steps: detection and association. They first detect all the objects from a single frame, where most of the methods also extract the corresponding appearance feature for each detected object for the later association. Early methods like [28, 36] deploy an extra appearance extraction network to obtain the representative object appearances. Recent methods such as [15, 31, 39] simply predict the appearance embedding along with the detection results from the same detector network.

For association, DeepSORT [32] proposes an association method that jointly utilizes the location overlaps and appearance affinity to obtain the matching results with the bipartite matching algorithms such as Hungarian Algorithm [13]. Many current methods such as [15, 31, 39] also apply such association method, using the probabilistic state estimation methods like Kalman Filter [12] to update the track state, which is hard to handle unexpected motions in a video. There are other methods taking different association strategies. [2] predicts the optical flow to merge the blobs, [5] uses graph to connect object nodes from different frames for association, [3] utilizes the previous detection results as region proposals to detect their associated objects at the current frame. These methods always require carefully designed rules to formulate the MOT association problem into their proposals to guarantee the effectiveness.

**Joint detection and tracking.** The joint detection and tracking methods [22, 23, 41] predict the association, along with the corresponding detections from adjacent frames. TubeTK [22] and ChainedTracker [23] predict the object locations with the same identity in the adjacent frames simultaneously. CenterTrack [41] estimates the detection results along with an offset vector, which indicates the motion information from the current object center to its center at the previous frame. Though with a simpler pipeline, such a joint detection and tracking paradigm overlooks the different focus of detection and association. Without a more explicit and reliable feature alignment mechanism for the object in adjacent frames as [44] in video object detection, the object features in more than one frame might disturb the detection on the single frame.

**Transformer in multi-object tracking.** Following the recently popular transformer-based detectors [6, 43], transformer is applied to solve the multi-object tracking problem.

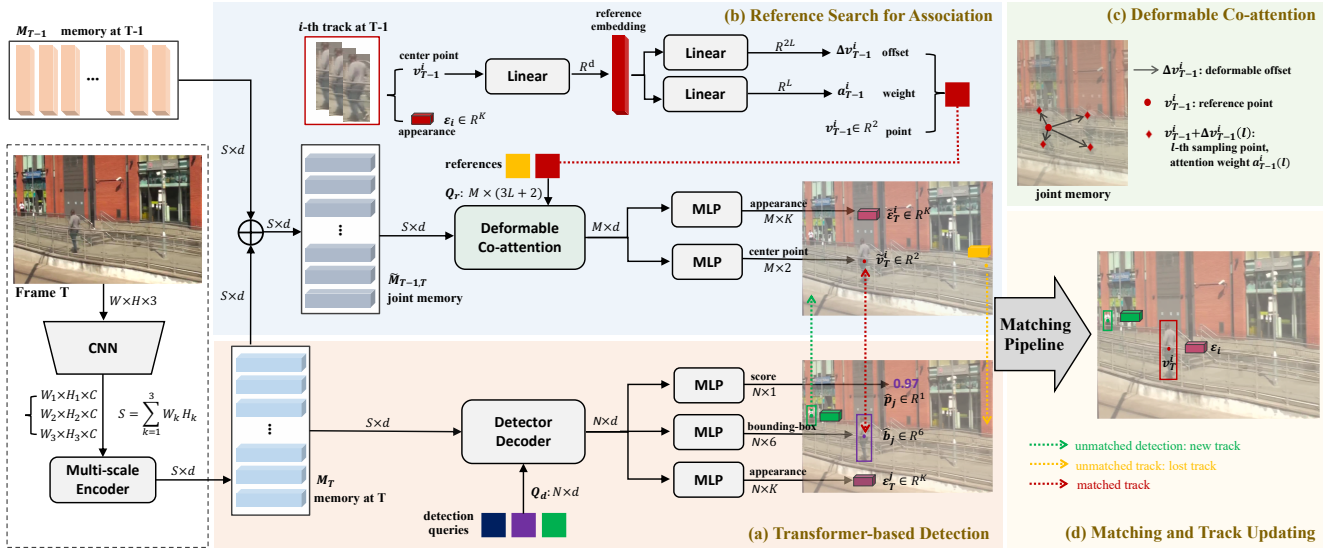


Figure 2. Overview of the proposed framework. (a): For tracking at frame  $T$ , we perform detection based on the features from frame  $T$  to obtain the object appearance embedding and the detection results. (b): The Reference Search (RS) module is deployed to predict states at frame  $T$  for the existing tracks at  $T - 1$ . The RS module takes the feature summation (joint memory) of frame  $T$  and  $T - 1$  as input. (c): The previous track locations are utilized as reference points to aggregate the corresponding features with deformable co-attention and make a one-to-one prediction of the state (appearance and location) for each track reference. (d): The predicted track states are associated with the new detections through a matching pipeline. Based on the matching results, previous tracks are finally updated at the frame  $T$ .

Some new tracking methods as [20,27,37] utilize object features from the previous frame to generate detection queries for the current frame. [35] uses the transformer with dense queries for tracking the target centers. Though the transformer has impressive detection performance and structure natural for the parallel association, the learned queries for transformer are highly specialized, which are hard to generalize on different tasks directly. Other methods like [7] designs graph transformers to model the spatial and temporal interactions among objects. However, it requires relationship modelling on each potentially associated node and thus costs more computation and memory.

### 3. TR-MOT

In this section, we introduce the Tracking-by-Reference MOT (TR-MOT), an online tracking framework as Fig 2, which decouples the detection and association process in multi-object tracking. Precisely, for detection, we deploy a transformer-based detector; for the association, we design the Reference Search (RS) module to predict the current state of each previous track by leveraging visual temporal information. We propose a corresponding matching pipeline to match the predicted states with newly detected objects and further update the tracks. Finally, a joint training strategy will be introduced to train the whole framework.

#### 3.1. Transformer-based Detection

Considering the impressive detection performance and set-to-set structure similar to our RS module, we apply

the efficient and fast-converging transformer-based detector, called Deformable DETR [43] for detection as Fig 2 (a). The detector contains an encoder and a decoder. Given the image at frame  $T$ , after the features are extracted by the backbone CNN, the detector encoder performs multi-scale deformable self-attention on each feature location to aggregate the feature memory  $M_T$ . Through the linear projections via  $N$  learnable queries  $Q_d$ , we obtain  $N$  reference points with their corresponding sampling offsets and attention weights respectively for the multi-scale deformable co-attention in the detector decoder. The decoder aggregates the corresponding features from  $M_T$  and decodes  $N$  object features for each query one-to-one. From each object feature, three separate heads based on multi-layer perceptrons (MLPs) are used to predict the object bounding-box, category score and appearance embedding, respectively.

Unlike the original deformable DETR, our detector needs to detect the objects even when their center points are outside the image. Thus, we modify deformable DETR for MOT. We clamp each center point into the image and predict the distances from the new center point to four bounding-box sides, respectively, instead of simply predicting the width and the height. For the appearance embedding prediction, we attach a multi-class classifier ( $\varphi$ ) to the embedding to predict the identity in the training since the ground-truth identity is known. In this way, we can pull the appearance embedding with the same identity altogether, making the embedding more discriminative and representative.

**Set-based training.** Considering the loss function should be invariant by a permutation of the prediction set, the Hungarian algorithm [13] is adopted to assign the ground-truth for supervision. Specifically, we find a one-to-one bipartite matching that minimizes the bounding-box overlap and category difference between the ground-truth  $y$  and the  $N$  detected objects  $\hat{y}$ . Denoting the predicted bounding-box, category scores and appearance embedding as  $\hat{b}_\sigma$ ,  $\hat{p}_\sigma$  and  $\hat{\varepsilon}_\sigma$  respectively, the detection loss  $\mathcal{L}_{\text{det}}$  for the  $i$ -th ground-truth object with an identity of  $\alpha$  is defined as:

$$\mathcal{L}_{\text{det}(i)} = \mathbb{1}_{\{c_i \neq \emptyset\}} [\lambda_{\text{box}} \mathcal{L}_{\text{box}}(b_i, \hat{b}_{\sigma(i)}) + \lambda_{\text{id}} \mathcal{L}_{\text{id}}(\alpha, \varphi(\hat{\varepsilon}_{\sigma(i)}))] + \lambda_{\text{cls}} \mathcal{L}_{\text{cls}}(c_i, \hat{p}_{\sigma(i)}),$$

where  $b_i$  and  $c_i$  denote the bounding-box and category of the  $i$ -th ground-truth respectively. The loss  $\mathcal{L}_{\text{box}}$  [43] is composed of a  $l_1$  loss and a GIoU loss, both the loss  $\mathcal{L}_{\text{cls}}$  and id loss  $\mathcal{L}_{\text{id}}$  are Focal Loss [16].

### 3.2. Reference Search for Association

We design a Reference Search (RS) module as Fig 2 (b) to predict the current state of previous tracks for the association, using the previous states as references. The appearance similarity and location distance can complement each other under crowded or occluded scenarios. Thus, we include both the location and appearance embedding into the track state.

We add  $M_{T-1}$  from the detection encoder at frame  $T-1$  to  $M_T$  at  $T$  to obtain the joint memory  $\tilde{M}_{T-1,T}$ . To aggregate the corresponding features for the track state prediction at frame  $T$ , we perform multi-scale deformable co-attention as Fig 2 (c) at the center point  $v_{T-1}$  of each track (reference point) at frame  $T-1$  based on  $\tilde{M}_{T-1,T}$ . A linear projection is used to transform  $v_{T-1}$  to the reference embedding, which is then used to generate the corresponding  $L$  location offsets  $\Delta v_{T-1} \in \mathbf{R}^{2L}$  and attention weights  $a_{T-1} \in \mathbf{R}^L$  for the adaptive deformable co-attention. After aggregating the  $\tilde{M}_{T-1,T}$  features at  $(v_{T-1} + \Delta v_{T-1})$  by the corresponding weights  $a_{T-1}$ , we apply two MLP heads to predict the center point location  $\tilde{v}_T$  at frame  $T$  and the appearance embedding  $\tilde{\varepsilon}_T$  for each previous track one-to-one.

The tracks with  $v_{T-1}$  outside the image region at frame  $T-1$  are not considered as references to our RS module. We consider their clamped  $v_{T-1}$  not the actual center points, and the extracted appearance for less than half body is unreliable to represent the object. Matching for RS is not applied between these tracks and the newly detected objects. The matching details will be described in the following contents.

**Training.** In this part, the goal of training is to make the RS module gain the ability to recognize the association between objects with the same identity from two adjacent frames. To this end, we only train the module when there exist object

pairs that can be associated. Given the  $i$ -th track at frame  $T-1$ , we denote its center point location at frame  $T-1$  as  $v_{T-1}^i$ , and the ground-truth center point location of the track at frame  $T$  as  $v_T^i$ . Using  $v_{T-1}^i$  as the reference points, we deploy the RS module to predict the center point location  $\tilde{v}_T^i$  and the appearance embedding  $\tilde{\varepsilon}_T^i$  for the  $i$ -th track at frame  $T$ . Then we calculate the L1 loss as  $\mathcal{L}_{\text{reg}}$  between  $\tilde{v}_T^i$  and the corresponding ground-truth  $v_T^i$  to supervise the location prediction for the center point. Similar to the detection part, we construct the id loss  $\mathcal{L}_{\text{id}}$  for supervision on the appearance embedding prediction. The RS training loss  $\mathcal{L}_{\text{RS}}$  on  $M$  references  $Q_r$  is defined as:

$$\mathcal{L}_{\text{RS}} = \sum_{i=1}^M [\lambda_{\text{reg}} \mathcal{L}_{\text{reg}}(v_T^i, \tilde{v}_T^i) + \lambda_{\text{id}} \mathcal{L}_{\text{id}}(\alpha, \varphi'(\tilde{\varepsilon}_T^i))] \quad (1)$$

**Multi-layer RS.** We construct the multi-layer RS for better performance, where each layer has the same structure. The aggregated features before MLP of each layer are utilized to update the reference embedding of the next layer. And  $\tilde{\varepsilon}_T$  is only predicted from the last layer. We apply the auxiliary losses [1] after each layer for supervision.

### 3.3. Matching and Track Updating

As Fig 2 (d), after predicting the current state for each track, a corresponding matching strategy is designed to associate the newly detected objects to the existing tracks.

**Matching for RS.** We assume a reliable state prediction from RS contains the appearance embedding consistent with the embedding of its corresponding track reference. Therefore, to assess the predicting reliability, we introduce Reference Consistency, which indicates the appearance similarity between the RS prediction and the reference.

Given the  $i$ -th track at frame  $T-1$ , we denote its appearance embedding as  $\varepsilon_i$  and the center point location as  $v_{T-1}^i$ . Besides the  $\tilde{v}_T^i$  and  $\tilde{\varepsilon}_T^i$  that are predicted from the RS module, we apply the Kalman Filter [12] to predict the shape  $(w_T^i, h_T^i)$  of the  $i$ -th track at frame  $T$ . In the detection process at frame  $T$ , for the  $j$ -th detected object, the predicted center point with the bounding box shape is denoted as  $\hat{l}_T^j = (\hat{v}_T^j, \hat{w}_T^j, \hat{h}_T^j)$ , and the appearance embedding is  $\hat{\varepsilon}_T^j$ . The RS matching cost between the  $i$ -th track and the  $j$ -th detected object consists of three parts: 1) the Euclidean distance between  $\tilde{l}_T^i = (\tilde{v}_T^i, w_T^i, h_T^i)$  and  $\hat{l}_T^j$ ; 2) the Reference Consistency between  $\varepsilon_i$  and  $\tilde{\varepsilon}_T^i$ ; 3) the appearance similarity between  $\tilde{\varepsilon}_T^i$  and  $\hat{\varepsilon}_T^j$ . We utilize the cosine similarity to calculate the Reference Consistency and appearance similarity. The RS matching cost  $\mathcal{C}_{RS}(i, j)$  between the  $i$ -th track and the  $j$ -th detected object is constructed as:

$$\mathcal{C}_{RS}(i, j) = \lambda_{\text{emb}} \sqrt{\frac{\varepsilon_i \cdot \tilde{\varepsilon}_T^i}{\|\varepsilon_i\| \|\tilde{\varepsilon}_T^i\|} \cdot \frac{\tilde{\varepsilon}_T^i \cdot \hat{\varepsilon}_T^j}{\|\tilde{\varepsilon}_T^i\| \|\hat{\varepsilon}_T^j\|}} + (1 - \lambda_{\text{emb}}) \|\tilde{l}_T^i - \hat{l}_T^j\| \quad (2)$$



**Matching pipeline.** The objects with detection scores over  $\mu$  are preserved for further association. First, we calculate  $\mathcal{C}_{RS}$  and find the bipartite matching with the least cost between the detections and the state predictions for previous tracks from RS. Only the matching that costs less than  $\tau$  is valid. Then we associate the remaining detected objects with the remaining previous tracks that have the most location overlaps, where the overlaps should be greater than a threshold of  $\theta$ . After these two steps, the previous tracks that are not associated are denoted as the lost tracks, and the remaining detected objects are considered as the new unconfirmed tracks. We confirm a new track only if it is associated with a detected object at the next frame, otherwise we will remove the track.

**Track updating.** The associated previous tracks apply the corresponding matched objects to update their locations and appearance embedding. To re-identify the lost tracks, we use the Kalman Filter [12] to update their states when the consecutive lost frames are less than  $\xi$ . Otherwise, the tracks are terminated and become inactive. After that, all the active tracks, including the active lost tracks, are taken as RS references at the next frame. The effectiveness of the re-identifying strategy for track rebirth is verified in Sec 4.4.

### 3.4. Joint Training

A joint training strategy is designed for our proposed framework. Two adjacent frames are taken as the input, and we perform detection on the two frames, respectively. To make the training process more robust and consistent to the inference, we take the detected objects from the previous frame  $T - 1$  as references for RS at the latter frame  $T$ . The loss function of our joint training is defined as:

$$\mathcal{L}(T) = 0.5(\mathcal{L}_{\text{det}}(T - 1) + \mathcal{L}_{\text{det}}(T)) + \mathcal{L}_{\text{RS}}(T - 1, T), \quad (3)$$

where  $\mathcal{L}(T)$  and  $\mathcal{L}(T - 1, T)$  indicate the loss functions based on frame  $T$  and the combination of frame  $T - 1$  with  $T$ , respectively. In the loss backpropagation process, we stop the gradient backpropagation of features from  $T - 1$ .

## 4. Experiments

### 4.1. Datasets and Metrics

**Datasets.** We verify the effectiveness of our method on two datasets, *i.e.*, MOT17 [21] and MOT20 [8]. MOT17 consists of 14 sequences with heavy occlusions, which are split into 7 sequences for training and 7 sequences for testing. MOT20 consists of 8 sequences depicting very crowded challenging scenes.

**Metrics.** We apply the official evaluation metrics in MOT datasets. 1) MOTA [4]: Summary of overall tracking accuracy in terms of false positives, false negatives and identity switches. 2) IDF1 [24]: The ratio of correctly identified detections over the average number of ground-truth and computed detections. 3) MOTP [4]: The misalignment between

the annotated and the predicted bounding boxes. 4) MT: Mostly tracked targets. The ratio of ground-truth trajectories that are covered by a track hypothesis for at least 80% of their respective life span. 5) ML: Mostly lost targets. The ratio of ground-truth trajectories that are covered by a track hypothesis for at most 20% of their respective life span. 3) HOTA [18]: Geometric mean of detection accuracy and association accuracy. Averaged across localization thresholds. 4) IDS [14]: Number of identity switches.

### 4.2. Implementation Details

We implement our detector following the setting of two-stage Deformable DETR with iterative bounding box refinement [43], utilizing 300 object queries and a ResNet-50 backbone [11].  $d$  and  $K$  in Fig 2 are 256 and 64 respectively. A 6-layer RS module is applied, where  $L$  is 12 in total for all three scales. For training, we first pretrain our model on the CrowdHuman dataset with the MOT17 or MOT20 dataset and then finetuning on these two datasets while blocking CrowdHuman for appearance embedding training. For the CrowdHuman dataset without annotated identities, we give each object a unique identity to train the appearance embedding branch in a self-supervised way following [39]. We first pretrain our model for 20 epochs with a learning rate of  $10^{-4}$ , and then finetune for 25 epochs with a learning rate of  $10^{-4}$  decreased by 10 times at the 20th epoch. For both the training steps, the batch size is 12, and the optimizer is AdamW [17]. We set the weight coefficients  $\lambda_{\text{reg}}$ ,  $\lambda_{\text{id}}$ ,  $\lambda_{\text{det}}$  and  $\lambda_{\text{RS}}$  in Sec 3 to 5, 0.5, 1 and 1 respectively. For inference, the hyper-parameters  $\mu$ ,  $\tau$ ,  $\theta$  and  $\xi$  in the matching pipeline are set to 0.4, 0.8, 0.5 and 30 respectively. All experiments are conducted on the GTX 1080Ti, CUDA 9.0.

### 4.3. Main Results

We conduct experiments on two benchmarks to verify our effectiveness. In Table 1, we compare our performance with the reported results of previous online methods. On MOT17, we achieve 76.5% on MOTA, 72.6% on IDF1 and 59.7% on HOTA, which outperform the state-of-the-art. Moreover, comparing to the methods [27, 35], which also adopt a Deformable DETR detector, our TR-MOT largely outperforms on IDF1 and HOTA by 9.1% and 5.2% respectively, and also outperforms on detection related metrics MOTA1 by 1.3%. On MOT20, we achieve 67.1% on MOTA, 59.1% on IDF1 and 50.4% on HOTA. In the extremely crowded MOT20 datasets, the appearance of each human is of relatively low quality and not easily to be differentiated. Some methods [15, 30, 39] use additional ReID datasets like [10, 34, 40] to train the appearance embedding branch with high-quality human appearances and clear identities, to further improve their association ability. Comparing to these methods on MOT20, our method without

Benchmark	Method	Detector	Extra Data	MOTA $\uparrow$	IDF1 $\uparrow$	HOTA $\uparrow$
MOT17	SST [28]	Faster R-CNN	$\times$	52.4	49.5	39.3
	Tracktor+Ctdet [3]	Faster R-CNN	$\times$	54.4	56.1	-
	DeepSORT [32]	Faster R-CNN	$\times$	60.3	61.2	-
	TubeTK [22]	3D FCOS	$\times$	63.0	58.6	48.0
	ChainedTracker [23]	RetinaNet	$\times$	66.6	57.4	49.0
	GSDT [30]	CenterNet	5D2	73.2	66.5	55.2
	FairMOT [39]	CenterNet	5D1	73.7	72.3	59.3
	CSTrack [15]	YOLOv5	5D1	74.9	72.6	59.3
	FUFET [25]	ResNet101-FPN	5D1	76.2	68.0	57.9
	CorrTracker [29]	CenterNet	5D1	76.5	73.6	60.7
	Centertrack [41]	CenterNet	CH	67.8	64.7	52.2
	TraDeS [33]	CenterNet	CH	69.1	63.9	52.7
	TransCenter [35]	Deformable-DETR	CH	73.2	62.2	54.5
	TransTrack [27]	Deformable-DETR	CH	75.2	63.5	54.1
TR-MOT (Ours)	Deformable-DETR	CH	76.5	72.6	59.7	
MOT20	FairMOT [39]	CenterNet	5D1	61.8	67.3	54.6
	CSTrack [15]	YOLOv5	5D1	66.6	68.6	54.0
	GSDT [30]	CenterNet	5D2	67.1	67.5	53.6
	TransCenter [35]	Deformable-DETR	CH	58.3	46.8	44.3
	TransTrack [27]	Deformable-DETR	CH	64.5	59.2	48.5
	TR-MOT (Ours)	Deformable-DETR	CH	67.1	59.1	50.4

Table 1. Performance comparison on the MOT17 and MOT20 test set with private detector. 5D1 indicates using 5 datasets, including CH [26], Caltech Pedestrian [9], CityPersons [38], CUHK-SYS [34], and PRW [40], 5D2 is 5D1 replacing CH by ETH [10]

utilizing any ReID dataset does not have superiority on association. However, we outperform other methods which use the the same datasets and detector as ours for training. The main results indicate that our performance boosts from our well designed MOT pipeline with the associating module RS, rather than only from the detector. We achieve competitive association ability while maintaining the high detection performance.

#### 4.4. Ablation Studies

For ablation studies, we first pretrain our model using CrowdHuman and finetune on the first half of MOT17 training set [39], following other settings introduced in the implementation details. Then we evaluate the trained models on the other half of MOT17 training set. We focus on three significant MOT metrics: MOTA, IDF1 and IDS. According to previous metrics definition, MOTA, IDS and IDF1 mainly indicate the detection performance, association stability, and association reliability, respectively. Considering most variants we implement mainly differ in the association process, we give priority to the metric IDF1.

**Baseline model.** For a fair comparison to verify the effectiveness of our proposed method, we follow JDE [31]

to implement a variant as our baseline model and replace the detector with the same Deformable DETR detector as ours. We simultaneously output detection results and the corresponding appearance embedding from the last decoder layer, then associate the detected objects with previous tracks based on appearance affinity and location distance.

**Proposed framework with RS.** We implement our proposed pipeline with a 3-layer RS module (+  $3 \times RS$  w/ *appearance*) and also a variant without learning the appearance embedding in the 3-layer RS module (+  $3 \times RS$  w/o *appearance*). As shown in Table 2a, we compare the results of these two variants with the baseline model on the validation sequences, respectively. Both two variants with our proposed RS module have comparatively superior performance on the sequence with a moving camera or under heavy occlusion. Especially, on the Video-05 and Video-11 which are with both heavy occlusion and apparent camera motion, +  $3 \times RS$  w/ *appearance* outperforms 20% and 67% relatively over the baseline model on the id association relevant metric IDF1, respectively. We consider it is because the baseline model does not leverage any visual temporal information like our RS module, which makes it not easier to handle unexpected erratic motions. Moreover, Table 2b

Variant	Video-02†	Video-04	Video-05*†	Video-09	Video-10*	Video-11*†	Video-13*
<i>Baseline Model, w/o RS</i>	42.8 / 42.1	82.3 / 85.7	59.3 / 65.7	74.8 / 78.8	65.6 / 61.2	45.9 / 68.1	82.0 / 65.2
+ 3× <i>RS w/o appearance</i>	43.8 / 44.8	82.2 / 86.7	75.3 / 69.3	74.1 / 79.1	60.7 / 61.0	61.8 / 69.4	71.7 / 61.8
+ 3× <i>RS w/ appearance</i>	46.5 / 46.0	84.1 / 85.7	71.0 / 67.2	70.7 / 78.9	71.0 / 63.3	76.7 / 68.6	79.8 / 62.6
+ 3× <i>RS w/o appearance</i> Δ	+2.3%/+6.4%	-0.1%/+1.2%	+27%/+5.5%	-0.9%/+0.4%	-7.5%/+0.3%	+35%/+1.9%	-12%/+5.2%
+ 3× <i>RS w/ appearance</i> Δ	+8.6%/+9.3%	+2.2%/+0.0%	+20%/+2.3%	-5.5%/+0.1%	+8.2%/+3.4%	+67%/+0.7%	-2.7%/+4.0%

(a) **Ablations on Sequences.** The value in the table indicates two important metrics IDF1 ↑ / MOTA↑ on the validation sequences. \* denotes the sequence shot by an apparently moving camera, and † means the validation sequence is crowded and with a heavy occlusion.

Variant	RS Layers	State Prediction	IDF1↑	MOTA↑	IDS↓	MT↑	ML↓	#Parameters
<i>Baseline, w/o RS</i>	-	Kalman Filter	69.1	70.8	382	161	50	41.0 M
+ <i>RS w/o appearance</i>	3×	Reference Search	70.7	72.0	607	<b>164</b>	51	44.7 M
+ <i>RS w/ appearance</i>	1×	Reference Search	73.5	<b>72.9</b>	321	152	51	42.6 M
	3×	Reference Search	74.2	71.9	287	160	<b>48</b>	44.9 M
	6×	Reference Search	<b>76.0</b>	72.5	<b>233</b>	162	51	48.3 M

(b) **Component Analysis:** Results of the variants with various components, *i.e.* The detection threshold  $\mu = 0.4$ , and RS matching cost threshold  $\tau = 1.5$ .

$\tau$	Matching Pipeline			IDF1 ↑	MOTA ↑	IDS ↓	Strategy				
	IDF1 ↑	MOTA ↑	IDS ↓				IDF1 ↑	MOTA ↑	IDS ↓		
0.5	73.6	70.8	656	<i>IoU + confirm</i>	63.4	69.1	910	<i>w/o</i>	75.0	72.1	375
				<i>JDE+IoU+confirm</i>	69.1	70.8	382				
0.8	<b>76.5</b>	72.4	278	<i>RS loc. matching</i>	61.0	69.3	1056	<i>average</i>	75.7	72.3	299
				<i>RS loc.+RS App.</i>	63.0	69.0	1131				
1.0	76.3	72.4	266	<i>Full RS (RS w/ lost ref)</i>	71.3	68.3	1681	<i>sqrt</i>	<b>76.5</b>	<b>72.4</b>	<b>278</b>
1.2	76.1	72.4	245	<i>Full RS + confirm</i>	74.9	70.8	616				
1.5	76.0	<b>72.5</b>	<b>233</b>	<i>(RS w/o lost ref)+IoU+confirm</i>	65.2	70.2	575				
1.8	75.0	72.4	238	<i>Full RS+IoU+confirm</i>	<b>76.5</b>	<b>72.4</b>	<b>278</b>				

(c) **Threshold of  $C_{RS}$ .**  $\mu = 0.4$ .

(d) **Matching Pipeline.**  $\tau = 0.8$ ,  $\mu = 0.4$ .

(e) **Reference Consistency Strategy.**  $\tau = 0.8$ ,  $\mu = 0.4$ .

Table 2. Ablation studies of our proposed model on the MOT17 validation set.

shows the variants with RS yield 1.6% - 6.9% and 1.1% - 2.1% improvements on IDF1 and MOTA respectively, comparing to the baseline model.

**Importance of RS appearance.** According to Table 2a, RS with appearance learning (+ 3× *RS w/ appearance*) outperforms the variant without appearance (+ 3× *RS w/o appearance*) in most sequences that are with heavy occlusion or camera motion. Table 2b shows + 3× *RS w/ appearance* gains a 3.5% improvement over + 3× *RS w/o appearance* on IDF1, and the IDS is dropped by 52.7% relatively over + 3× *RS w/o appearance* when RS appearance learning is involved. We consider the appearance embedding obtained from our RS module is more representative by leveraging the temporal information. Since the RS module mainly contributes to the association, the detection relevant metric MOTA is less affected. With a relative similar detection performance, the apparent improvement on IDF1 and dropping on IDS can verify the effectiveness of the RS appearance for a more stably accurate association.

**Number of Reference Search layers.** We construct a multi-layer RS structure in our TR-MOT. As shown in Table 2b, row 3 - 5, IDF1 is improved by 2.5% from 1 layer to 6 layers, and IDS is dropped from 321 to 233 in a stable way. The improvements of IDF1 and dropping of IDS along with the close detection performance can verify our RS module with more layers can benefit the association performance.

**Matching cost for RS.** During the matching for RS, we

calculate the matching cost  $C_{RS}$  through Sec 3.3. Based on our optimal model structure with a 6-layer RS module (+ 6× *RS w/ appearance*), we set the maximum threshold  $\tau$  of  $C_{RS}$  from 0.5 to 1.8 and keep all other settings following 4.2 to perform the sensitivity analysis on  $\tau$ . As shown in Table 2c, IDF1 improves by 2.9% when  $\tau$  changes from 0.5 to 0.8, drops by only 0.5% when  $\tau$  increases from 0.8 to 1.5, and drops by 1.0% as  $\tau$  changes from 1.5 to 1.8. Moreover, the detection relevant metric MOTA keeps almost unchanged when  $\tau$  is from 0.8 to 1.8. Table 2c shows the association performance has consistent effectiveness when  $\tau$  is set from 0.8 to 1.5, and is best when  $\tau = 0.8$ . When  $\tau$  is smaller, the matching for RS will be more strict and thus results in more unreliable new tracks to be unconfirmed and removed. Therefore, the detection recall will drop and degrade the detection relevant metric MOTA, which explains the 1.6% dropping on MOTA when  $\tau$  decreases from 0.8 to 0.5.

**Matching for RS.** Rows 3 - 5 in Table 2d show the ablations on the matching for RS. When lost tracks are excluded from the references and only RS matching is utilized, involving RS appearance into the RS matching cost (*RS loc.+RS App.*) can improve IDF1 by 2% with very close MOTA comparing to only considering the updated track location from RS (*RS loc. matching*). It verifies the association effectiveness of jointly considering RS appearance and location overlaps in the matching process for RS.

**Strategy for Reference Consistency.** According to Sec

3.3, we introduce Reference Consistency to assess the reliability of RS predictions. As Table 2e, we implement two strategic variants for involving the Reference Consistency to RS matching. When calculating the RS matching cost, if we take the average value of the Reference Consistency and appearance similarity (*average*), IDF1 and MOTA will drop by 0.8% and 0.1%, respectively, comparing to taking the sqrt value. If we exclude the Reference Consistency, IDF1 and MOTA will further drop by 0.7% and 0.2% respectively comparing to *average*. Therefore, Table 2e verifies the contribution of our proposed Reference Consistency.

**Rebirth in RS.** If we add the lost tracks into the track references (*Full RS (RS w/ lost ref)*) based on *RS loc. Matching*, IDF1 will be improved largely by 8.3%, although MOTA drops by 0.7%. However, *Full RS+IoU+confirm* improves IDF1 by 11.3% over (*RS w/o lost ref*)+*IoU+confirm* while MOTA increases by 2.2% and IDS drops by 297. Without the *confirm* process, more lost tracks in low quality as references will impair the RS matching and increase the IDS, which degrades the metric MOTA and IDF1. When we involve *confirm* based on *Full RS (RS w/ lost ref)*, *Full RS + confirm* will improve IDF1 and MOTA by 3.6% and 2.5%, respectively. These ablations indicate that considering the lost tracks in RS for track rebirth is necessary, and also the performance benefits from the *confirm* process.

**Matching pipeline.** For the full matching pipeline (*Full RS+IoU+confirm*), we perform matching for RS (*full RS*), and deploy matching for the location overlaps (*IoU*) to associate the remaining detected objects and tracks. Moreover, the unconfirmed tracks that are not associated to new detections will be removed (*confirm*). To verify the effectiveness of our designed matching pipeline with RS, we implement several variants while keeping the hyperparameters. If we exclude *full RS* for matching (*IoU+confirm*), IDF1 drops greatly by 13.1% and MOTA also drops by 3.3%. If we replace *full RS* to the matching strategy based on the appearance embedding and detection results from the detector as JDE [31] (*JDE*), IDF1 drops by 7.4% and MOTA drops by 1.6%. These two ablations verify the large contribution to the association is from our *full RS* in the matching pipeline. Overall, our designed matching pipeline (*Full RS+IoU+confirm*) can achieve the best result.

#### 4.5. Visualization

As shown in Fig 3, we visualize the attention of our detector on one frame (a) and RS attention on two adjacent frames (b) in (+ 6 × RS w/ appearance). From the figure, the detector focuses more on the keypoints of the human body to predict an accurate human location. Differently, our RS module concerns features of both humans that are associated with each other, especially the aligned body features from adjacent frames near the reference locations. Some contexts are also taken into account by the RS module for

a more reliable association. The visualization indicates our RS module can cognize the appearance feature alignment for each track between adjacent frames. It also explains why the predicted appearance embedding from RS is more representative and thus benefits the association process.



Figure 3. Visualization for the detector attention and RS attention. The sub-figures in (a) and (b) have a one-to-one correspondence. The yellow cross in sub-figure (a) indicates the reference location of RS in the corresponding sub-figure (b).

## 5. Conclusion

In this paper, we propose an effective online MOT framework TR-MOT. Specifically, we design a Reference Search module for more reliable association, which takes previous tracks as references to predict the current state for each track reference, based on the visual temporal information. Compatibly, We propose an effective matching pipeline to associate new detections with the predicted track states and then update the existing tracks. Moreover, we introduce a joint training strategy for the end-to-end training. Our method achieves competitive performance on the MOT dataset.

## References

- [1] Rami Al-Rfou, Dokook Choe, Noah Constant, Mandy Guo, and Llion Jones. Character-level language modeling with deeper self-attention. In *AAAI*, 2019. 4
- [2] David-Alexandre Beaupré, Guillaume-Alexandre Bilodeau, and Nicolas Saunier. Improving multiple object tracking with optical flow and edge preprocessing. *CoRR*, abs/1801.09646, 2018. 2
- [3] Philipp Bergmann, Tim Meinhardt, and Laura Leal-Taixe. Tracking without bells and whistles. In *ICCV*, 2019. 2, 6
- [4] Keni Bernardin and Rainer Stiefelhagen. Evaluating multiple object tracking performance: the clear mot metrics. *EURASIP Journal on Image and Video Processing*, 2008. 5
- [5] Guillem Brasó and Laura Leal-Taixé. Learning a neural solver for multiple object tracking. In *CVPR*, 2020. 2
- [6] Nicolas Carion, Francisco Massa, Gabriel Synnaeve, Nicolas Usunier, Alexander Kirillov, and Sergey Zagoruyko. End-to-end object detection with transformers. In *ECCV*, 2020. 2
- [7] Peng Chu, Jiang Wang, Quanzeng You, Haibin Ling, and Zicheng Liu. Transmot: Spatial-temporal graph transformer



- for multiple object tracking. *CoRR*, abs/2104.00194, 2021. 3
- [8] Patrick Dendorfer, Hamid Rezatofighi, Anton Milan, Javen Shi, Daniel Cremers, Ian D. Reid, Stefan Roth, Konrad Schindler, and Laura Leal-Taixé. MOT20: A benchmark for multi object tracking in crowded scenes. *CoRR*, abs/2003.09003, 2020. 5
- [9] Piotr Dollár, Christian Wojek, Bernt Schiele, and Pietro Perona. Pedestrian detection: A benchmark. In *CVPR*, pages 304–311. IEEE, 2009. 6
- [10] Andreas Ess, Bastian Leibe, Konrad Schindler, and Luc Van Gool. A mobile vision system for robust multi-person tracking. In *CVPR*, pages 1–8. IEEE, 2008. 5, 6
- [11] Kaiming He, Xiangyu Zhang, Shaoqing Ren, and Jian Sun. Deep residual learning for image recognition. In *CVPR*, 2016. 5
- [12] R. Kalman. A new approach to linear filtering and prediction problems, transaction of the asme journal of basic. 1960. 2, 4, 5
- [13] H. W. Kuhn. The hungarian method for the assignment problem. In *Naval Research Logistics Quarterly*, 1955. 2, 4
- [14] Yuan Li, Chang Huang, and Ram Nevatia. Learning to associate: Hybridboosted multi-target tracker for crowded scene. In *CVPR*, 2009. 5
- [15] Chao Liang, Zhipeng Zhang, Yi Lu, Xue Zhou, Bing Li, Xiyong Ye, and Jianxiao Zou. Rethinking the competition between detection and reid in multi-object tracking. *arXiv preprint arXiv:2010.12138*, 2020. 1, 2, 5, 6
- [16] Tsung-Yi Lin, Priya Goyal, Ross Girshick, Kaiming He, and Piotr Dollár. Focal loss for dense object detection. In *ICCV*, 2017. 4
- [17] Ilya Loshchilov and Frank Hutter. Decoupled weight decay regularization. In *ICLR*, 2018. 5
- [18] Jonathon Luiten, Aljosa Osep, Patrick Dendorfer, Philip H. S. Torr, Andreas Geiger, Laura Leal-Taixé, and Bastian Leibe. HOTA: A higher order metric for evaluating multi-object tracking. *International Journal of Computer Vision*, 129(2):548–578, Oct 2020. 5
- [19] Nima Mahmoudi, Seyed Mohammad Ahadi, and Mohammad Rahmati. Multi-target tracking using cnn-based features: Cnnmtt. *Multimedia Tools and Applications*, 2019. 2
- [20] Tim Meinhardt, Alexander Kirillov, Laura Leal-Taixe, and Christoph Feichtenhofer. Trackformer: Multi-object tracking with transformers. *arXiv preprint arXiv:2101.02702*, 2021. 2, 3
- [21] Anton Milan, Laura Leal-Taixé, Ian Reid, Stefan Roth, and Konrad Schindler. Mot16: A benchmark for multi-object tracking. *arXiv preprint arXiv:1603.00831*, 2016. 5
- [22] Bo Pang, Yizhuo Li, Yifan Zhang, Muchen Li, and Cewu Lu. Tubetk: Adopting tubes to track multi-object in a one-step training model. In *CVPR*, 2020. 1, 2, 6
- [23] Jinlong Peng, Changan Wang, Fangbin Wan, Yang Wu, Yabiao Wang, Ying Tai, Chengjie Wang, Jilin Li, Feiyue Huang, and Yanwei Fu. Chained-tracker: Chaining paired attentive regression results for end-to-end joint multiple-object detection and tracking. In *ECCV*, 2020. 1, 2, 6
- [24] Ergys Ristani, Francesco Solera, Roger Zou, Rita Cucchiara, and Carlo Tomasi. Performance measures and a data set for multi-target, multi-camera tracking. In *ECCV*, 2016. 5
- [25] Chaobing Shan, Chunbo Wei, Bing Deng, Jianqiang Huang, Xian-Sheng Hua, Xiaoliang Cheng, and Kewei Liang. Tracklets predicting based adaptive graph tracking, 2020. 6
- [26] Shuai Shao, Zijian Zhao, Boxun Li, Tete Xiao, Gang Yu, Xiangyu Zhang, and Jian Sun. Crowdhuman: A benchmark for detecting human in a crowd. *arXiv preprint arXiv:1805.00123*, 2018. 6
- [27] Peize Sun, Yi Jiang, Rufeng Zhang, Enze Xie, Jinkun Cao, Xinting Hu, Tao Kong, Zehuan Yuan, Changhu Wang, and Ping Luo. Transtrack: Multiple-object tracking with transformer. *arXiv preprint arXiv:2012.15460*, 2020. 2, 3, 5, 6
- [28] ShiJie Sun, Naveed Akhtar, HuanSheng Song, Ajmal Mian, and Mubarak Shah. Deep affinity network for multiple object tracking. *TPAMI*, 2019. 1, 2, 6
- [29] Qiang Wang, Yun Zheng, Pan Pan, and Yinghui Xu. Multiple object tracking with correlation learning, 2021. 6
- [30] Yongxin Wang, Kris Kitani, and Xinshuo Weng. Joint object detection and multi-object tracking with graph neural networks, 2021. 5, 6
- [31] Zhongdao Wang, Liang Zheng, Yixuan Liu, and Shengjin Wang. Towards real-time multi-object tracking. *arXiv preprint arXiv:1909.12605*, 2019. 2, 6, 8
- [32] Nicolai Wojke, Alex Bewley, and Dietrich Paulus. Simple online and realtime tracking with a deep association metric. In *ICIP*, 2017. 1, 2, 6
- [33] Jialian Wu, Jiale Cao, Liangchen Song, Yu Wang, Ming Yang, and Junsong Yuan. Track to detect and segment: An online multi-object tracker, 2021. 6
- [34] Tong Xiao, Shuang Li, Bochao Wang, Liang Lin, and Xiaogang Wang. Joint detection and identification feature learning for person search. In *CVPR*, pages 3415–3424, 2017. 5, 6
- [35] Yihong Xu, Yutong Ban, Guillaume Delorme, Chuang Gan, Daniela Rus, and Xavier Alameda-Pineda. Transcenter: Transformers with dense queries for multiple-object tracking. *CoRR*, abs/2103.15145, 2021. 2, 3, 5, 6
- [36] Fengwei Yu, Wenbo Li, Quanquan Li, Yu Liu, Xiaohua Shi, and Junjie Yan. Poi: Multiple object tracking with high performance detection and appearance feature. In *ECCV*, 2016. 2
- [37] Fangao Zeng, Bin Dong, Tiancai Wang, Cheng Chen, Xiangyu Zhang, and Yichen Wei. Motr: End-to-end multiple-object tracking with transformer, 2021. 2, 3
- [38] Shanshan Zhang, Rodrigo Benenson, and Bernt Schiele. Citypersons: A diverse dataset for pedestrian detection. In *CVPR*, pages 3213–3221, 2017. 6
- [39] Yifu Zhang, Chunyu Wang, Xinggang Wang, Wenjun Zeng, and Wenyu Liu. Fairmot: On the fairness of detection and re-identification in multiple object tracking. *arXiv e-prints*, pages arXiv–2004, 2020. 2, 5, 6
- [40] Liang Zheng, Hengheng Zhang, Shaoyan Sun, Manmohan Chandraker, Yi Yang, and Qi Tian. Person re-identification in the wild. In *CVPR*, pages 1367–1376, 2017. 5, 6

- [41] Xingyi Zhou, Vladlen Koltun, and Philipp Krähenbühl. Tracking objects as points. In *ECCV*, 2020. [2](#), [6](#)
- [42] Zongwei Zhou, Junliang Xing, Mengdan Zhang, and Weiming Hu. Online multi-target tracking with tensor-based high-order graph matching. In *ICPR*, 2018. [2](#)
- [43] Xizhou Zhu, Weijie Su, Lewei Lu, Bin Li, Xiaogang Wang, and Jifeng Dai. Deformable detr: Deformable transformers for end-to-end object detection. In *ICLR*, 2020. [2](#), [3](#), [4](#), [5](#)
- [44] Xizhou Zhu, Yujie Wang, Jifeng Dai, Lu Yuan, and Yichen Wei. Flow-guided feature aggregation for video object detection. In *ICCV*, 2017. [2](#)